# Light baryon spatial correlators at short distances

Chao Han[*] and Jialu Zhang[†]

*INPAC, Key Laboratory for Particle Astrophysics and Cosmology (MOE), Shanghai Key Laboratory for Particle Physics and Cosmology, School of Physics and Astronomy, Shanghai Jiao Tong University, Shanghai 200240, China*

(Received 7 November 2023; accepted 6 January 2024; published 30 January 2024)

To study the light baryon light cone distribution amplitudes (LCDAs), the spatial correlator of the light baryon has been calculated up to one-loop order in coordinate space. They reveal certain identities that do not appear in the study of mesons DAs and parton distribution functions. Subsequently, it was renormalized using the ratio renormalization scheme involving division by a 0-momentum matrix element. Then through the matching in the coordinate space, the light baryon light cone correlator can be extracted out from the spatial correlator. These results provide insights into both the ultraviolet and infrared structures of the light baryon spatial correlator, which is valuable for further exploration in this field. Furthermore, the employed ratio scheme is an efficient and lattice-friendly renormalization approach suitable for short-distance applications. These can be used for studying the light baryon LCDAs using lattice techniques.

DOI: 10.1103/PhysRevD.109.014034

## I. INTRODUCTION

Light cone distribution amplitudes (LCDAs) for light baryons serve as fundamental components in the description of these light baryons. They are defined through the QCD factorization for the exclusive process with a large momentum transfer, and encodes the crucial nonperturbative physics within the light baryons [1]. They encapsulate vital nonperturbative information inherent to light baryons. These distribution amplitudes hold a key position in unraveling the inner structures of light baryons. They essentially outline how longitudinal momentum is distributed among the partons within a light baryon's leading Fock state. Alongside parton distribution functions (PDFs), which detail the parton distribution within baryons, they jointly provide a comprehensive description of baryonic structure. Moreover, light baryon LCDAs also play a important role in both standard model investigations [2] and explorations of new physics [3–5].

Despite their significance, light baryon LCDAs have not gained as much attention as PDFs. The primary challenge stems from the fact that in an exclusive process, several LCDAs through the convolution integrals enter the same physical observable. Additionally, for light baryons, their LCDAs are dependent on two variables, setting them apart from the more straightforward investigations of PDFs and meson DAs cases.

Historically, researches on light baryon LCDAs have predominantly relied on QCD sum rules [6–9] and lattice QCD [10–13]. Given their inherent nonperturbative nature, the results are model dependent and entail uncontrollable uncertainties. Consequently, only the lowest moments have been obtained [11–13].

In recent papers [14,15], large momentum effective theory (LaMET) [16–19] was adopted to study light baryon LCDA from the first principle through lattice QCD. LaMET has been employed to investigate various quantities, including PDFs [20–46], meson LCDAs [47–56], Transverse momentum dependent parton distributions (TMDs) [57–72], Generalized parton distributions (GPDs) [73–83], Light front wave functions (LFWFs) [84], Transverse momentum dependent wave functions (TMDWFs) [85–88], and Double parton distributions (DPDs) [89,90], demonstrating its capability in the study of light cone quantities. For more papers on the content and applications of LaMET, please refer to [18,91,92] and the references therein. In paper [14], the calculation was performed in momentum space, and the corresponding quasi-DA was renormalized using the Regularization-independent momentum subtraction scheme (RI/MOM) scheme. However, despite it is adoptable theoretically, the application of this scheme on the lattice introduced uncontrollable infrared effects. To address theses issues, we have developed a hybrid renormalization scheme specifically designed to handle the spatial correlator's divergences in different coordinate regions [15].

[*]chaohan@sjtu.edu.cn
[†]elpsycongr00@sjtu.edu.cn

However, throughout the entire process, the spatial correlator has not been comprehensively introduced with regard to its structures. To address this gap, this paper focuses on a detailed one-loop analysis of the spatial correlators of light baryons. In conjunction with the introduction of the calculation processes, this paper will also introduce the relevant ultraviolet (UV) and infrared (IR) structures inherent in the correlators. In this paper, the spatial correlators will be renormalized using the ratio scheme, which involves renormalizing spatial correlations by dividing by their own 0-momentum matrix element [93–95]. Besides, by employing the Ioffe-time distribution definition, the light cone correlator and spatial correlator can be studied on an equal footing. After that, we will perform the matching between the spatial correlator and light cone correlator directly on the coordinate space. Then the LCDAs can be obtained by performing the Fourier transformation upon the light cone correlator. The renormalization group equation (RGE) for the LCDA is also provided, and their connections with spatial correlator are discussed.

The rest of the paper is arranged as follows. Section II covers the essential content related to LCDAs and spatial correlators. Section III is dedicated to the calculation of one-loop results, where we present the patterns involved in spatial correlation calculations and analyze their UV and IR structures. Section IV focuses on the renormalization process through the ratio scheme, followed by matching. Additionally, we provide the scaling behavior of the LCDA for comparison with previous results as a validation check. The paper is summarized in the last section.

## II. LIGHT CONE DISTRIBUTION AMPLITUDES AND SPATIAL CORRELATORS FOR A LIGHT BARYON

In this section, we introduce the requisite notations and conventions required for subsequent discussions. In particular, the definition of LCDAs and Ioffe-time distribution (ITD) will be given. We start with the LCDAs, which are defined as the hadron-to-vacuum matrix elements of nonlocal operators consisting of quarks and gluon which live on the light cone. In the case of a light baryon, the three-quark matrix element can be constructed as [8]

$$\langle 0|\varepsilon^{ijk}u_\alpha^{i'}(z_1)U_{i'i}(z_1,z_0)d_\beta^{j'}(z_2)U_{j'j}(z_2,z_0)s_\gamma^{k'}(z_3) \times U_{k'k}(z_3,z_0)|\Lambda(P,\lambda)\rangle, \tag{1}$$

where $|\Lambda(P,\lambda)\rangle$ stands for the $\Lambda$ baryon state with the momentum $P$, $P^2=0$ and the helicity $\lambda$. $\alpha$, $\beta$, and $\gamma$ are Dirac indices. $i^{(\prime)}$, $j^{(\prime)}$, and $k^{(\prime)}$ denote color charges. In this paper, two light cone unit vectors are defined as $n^\mu=(1,0,0,-1)/\sqrt{2}$ and $\bar{n}^\mu=(1,0,0,1)/\sqrt{2}$. The momentum of the baryon is along the $\bar{n}$ direction, $P^\mu=P^+\bar{n}^\mu=(P^z,0,0,P^z)$. The coordinates are set in the $n$ direction, $z_i^\mu=z_i n^\mu$. The Wilson lines $U(x,y)$

$$U(x,y)=\mathcal{P}\exp\left[ig\int_0^1 \mathrm{d}t(x-y)_\mu A^\mu(tx+(1-t)y)\right] \tag{2}$$

are inserted to preserve the gauge invariance. For simplicity and brevity, we will choose $z_0=0$. Besides, the Wilson lines, color indexes, and helicity will not be written out explicitly below.

Based on Lorentz invariance, and the spin and parity requirement, the matrix element can be decomposed in terms of three functions, $V(z_iP\cdot n)$, $A(z_iP\cdot n)$, and $T(z_iP\cdot n)$ to the leading twist

$$\langle 0|u_\alpha(z_1)d_\beta(z_2)s_\gamma(z_3)|\Lambda(P)\rangle \tag{3}$$

$$=f_N\{(\not{P}C)_{\alpha\beta}(\gamma_5 u_\Lambda)_\gamma V(z_iP\cdot n) \tag{4}$$

$$+(\not{P}\gamma_5 C)_{\alpha\beta}(u_\Lambda)_\gamma A(z_iP\cdot n) +(i\sigma_{\mu\nu}P^\nu C)_{\alpha\beta}(\gamma_\mu\gamma_5 u_\Lambda)_\gamma T(z_iP\cdot n)\}, \tag{5}$$

where $C$ signifies the charge conjugation. $u_\Lambda$ stands for the $\Lambda$ baryon spinor. Equivalently, the three leading twist functions can be projected by inserting a specific gamma matrix $\Gamma$ into the $u$ and $d$ quark fields. In the following discussion, we will take $A(z_iP\cdot n)$ as an example while the other matrix elements can be similarly analyzed. Then we have

$$\begin{aligned}\tilde{\mathcal{I}}(z_1,z_2,z_3,P^+,\mu)&=\langle 0|\psi_1^T(z_1)\Gamma\psi_2(z_2)\psi_3(z_3)|\Lambda(P)\rangle_R,\\ &\quad\Phi_L(x_1,x_2,\mu)f_\Lambda(\mu)P^+u_\Lambda(P)\\ &=\int_{-\infty}^{+\infty}\frac{dP^+z_1}{2\pi}\frac{dP^+z_2}{2\pi}e^{ix_1P^+z_1+ix_2P^+z_2}\tilde{\mathcal{I}}(z_1,z_2,0,P^+,\mu),\end{aligned} \tag{6}$$

where $T$ means transpose and $\Gamma=C\gamma_5\not{n}$. $R$ stands for renormalization. $x_i$s label the longitudinal momentum fractions carried by the three quarks and $0\le x_i\le 1$. The $\mu$ denotes the renormalization scale which will be converted to the factorization scale when the factorization of quasi-DA is established. $f_\Lambda(\mu)$ is the $\Lambda$ baryon decay constant defined as follows $f_\Lambda(\mu)P^+u_\Lambda(P)=\tilde{\mathcal{I}}(0,0,0,P^+,\mu)$. Note that $f_\Lambda(\mu)$ depends on the renormalization scale $\mu$ since the local operator here is not a conserved current. The LCDA $\Phi_L(x_1,x_2,\mu)$ in Eq. (6) is dimensionless and normalized.

For the lattice QCD side, in order to extract the LCDA, the first step involves selecting an appropriate spatial correlator. In this paper, the spatial correlator is chosen as [8]

$$\tilde{M}(z_1, z_2, z_3, P^z, \mu) = \langle 0|u^T(z_1)\tilde{\Gamma}d(z_2)s(z_3)|\Lambda(P)\rangle_R, \quad (7)$$

where $\tilde{\Gamma} = C\gamma_5 \not{n}_z$. And the coordinates are set as $z_i^\mu = z_i n_z^\mu$, where $n_z^\mu = (0, 0, 0, 1)$.

These two kinds of correlators can be treated in a more unified manner. The light cone correlator can be understood as a function of two Lorentz-invariant arguments, $z_i P \cdot n$ and $z^2$. It has been extended to distributions beyond those lying on the light cone and is referred to as ITD [95,96]. The ITD is dependent on two Lorentz scalars, Ioffe time $\nu_i$ (defined as $-z_i P \cdot n_i$) and distance $z_i^2$, where the specific values of $n_i$ rely on our requirements. Consequently, we can represent the light cone correlator and spatial correlator as

$$\begin{aligned} \mathfrak{F}(z_1, z_2, z_3, P^+, \mu) &\equiv \mathfrak{F}(\nu_1, \nu_2, \nu_3, z^2, \mu), \\ \mathfrak{M}(z_1, z_2, z_3, P^z, \mu) &\equiv \mathfrak{M}(\nu_1, \nu_2, \nu_3, z^2, \mu), \end{aligned} \quad (8)$$

with $z^2$ being an expression compactly representing all possible contractions of the $z_i$ terms. It should be noted that, for the spatial correlator, only the leading twist component will be retained, which means that we will only keep the part that is proportional to $P^\mu$.

To establish a connection between the LCDAs and spatial correlators, in contrast to previous approaches, we directly extract the LC correlator by matching it with the spatial correlator in coordinate space. Subsequently, the light cone correlator can be Fourier transformed into LCDAs.

## III. ONE-LOOP CALCULATION OF THE SPATIAL CORRELATOR IN COORDINATE SPACE

In this section, the one-loop results for the spatial correlator and the light cone correlator will be presented. These results will be presented in dimensional regularization with $\overline{\text{MS}}$ renormalization. We will stick to adopt the Feynman gauge throughout, though the results are gauge invariant. All the calculation will be performed on the operator level. By following this approach, the desired matrix elements can be obtained by incorporating suitable out-states. As shown in Fig. 1, there are 12 distinct diagrams to calculate, which can be divided into three categories: quark-quark (q-q), quark-Wilson line (q-W), and Wilson line-Wilson line (W-W). We will begin with the q-W pattern, which exhibits the most complex structures among all three patterns. In the q-W pattern, there are two different situations to consider: cases (e), (f), (h), and (i), and cases (d) and (g).

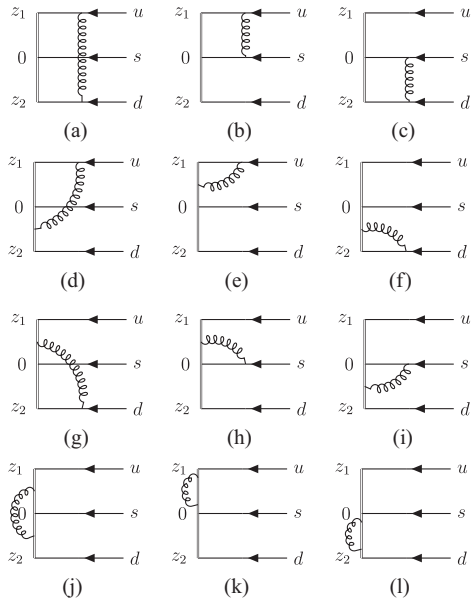


FIG. 1. One loop corrections for the equal-time matrix element of the $\Lambda$ baryon.

### A. q-W pattern

#### 1. Cases (e), (f), (h), and (i)

We take Fig. 1(e) as the example to illustrate the calculation, in which the one-loop corrections are

$$\tilde{O}_e = \left(\psi_1(z_1)\left(ig_s\int d^d\eta_1 \bar{\psi}_1(\eta_1)\not{A}(\eta_1)\psi_1(\eta_1)\right)\right)^T\left(-ig_s\int_0^1 dt_1 z_1\cdot A(t_1 z_1)\right)\tilde{\Gamma}\psi_2(z_2)\psi_3(0). \quad (9)$$

The color indexes and the parameter $(\frac{\mu^2}{e^{\ln(4\pi)-\gamma_E}})^\epsilon$ are not written out explicitly. The gluon and quark propagators in the coordinate space are

$$G(x-y) = \frac{\Gamma(d/2-1)}{4\pi^{d/2}}\frac{-g_{\mu\nu}}{(-(x-y)^2+i\epsilon)^{d/2-1}}, \qquad Q(x-y) = \frac{\Gamma(d/2)}{2\pi^{d/2}}\frac{i(\not{x}-\not{y})}{(-(x-y)^2+i\epsilon)^{d/2}}. \quad (10)$$

Following the standard routine, substituting them back and rearranging the formula, one arrives at

$$\tilde{O}_e = g_s^2 \frac{(-i)^{d/2-1}}{8\pi^{d/2}} \int d^d k_1 \int_0^1 dt_1 \int_0^\infty d\sigma_1 \int_0^\infty d\sigma_2 \sigma_1^{d/2-1} \sigma_2^{d/2-2} (\sigma_1+\sigma_2)^{-d/2} \times e^{\frac{i(4(\sigma_1+\sigma_2 t_1) z_1 (k_1\cdot n_z) + k_1^2 - 4\sigma_1\sigma_2(t_1-1)^2(-z_1^2))}{4(\sigma_1+\sigma_2)}} \psi_1^T(k_1) \left( (-z_1^2) - \frac{z_1(k_1\cdot n_z) + (\sigma_1+\sigma_2 t_1)(-z_1^2)}{\sigma_1+\sigma_2} \right) \tilde{\Gamma} \psi_2(z_2)\psi_3(0), \tag{11}$$

where $\sigma_1$ and $\sigma_2$ are Schwinger parameters, and $k_1$ is from the Fourier transformation of $\psi_1^T(z_1)$. Note that terms like $k_1^2$ or $\not{k}_1\psi(z)$ have been neglected in the calculation due to the equation of motion. By changing $(\sigma_1,\sigma_2)$ to $(\sigma,\eta)$ with $\sigma_1 = \frac{\sigma}{\eta}$ and $\sigma_2 = \frac{\sigma}{1-\eta}$, the above result can be rearranged as

$$\tilde{O}_e = \tilde{O}_{e1} + \tilde{O}_{e2}, \tag{12}$$

$$\tilde{O}_{e1} = -g_s^2 \frac{1}{8\pi^{d/2}} \Gamma(d/2-1) \int d^d k_1 \int_0^1 dt_1 \int_0^1 d\eta (1-t_1)^{3-d} (z_1^2)^{2-d/2} \tag{13}$$

$$\times e^{iz_1 k_1 (\eta(t_1-1)+1)} \psi_1^T(k_1) \tilde{\Gamma} \psi_2(z_2)\psi_3(0), \tag{14}$$

$$\tilde{O}_{e2} = -g_s^2 \frac{(-i)^{d/2-1}}{8\pi^{d/2}} \int d^d k_1 \int_0^1 dt_1 \int_0^1 d\eta \int_0^\infty d\sigma \sigma^{\frac{d}{2}-3} (1-\eta) z_1 (k_1\cdot n_z) \tag{15}$$

$$\times e^{-iz_1 n_z\cdot(k_1(-(\eta(t_1-1))-1)+\sigma(t_1-1)^2 z_1 n_z)} \psi_1^T(k_1) \tilde{\Gamma} \psi_2(z_2)\psi_3(0), \tag{16}$$

and then one can separate it into two parts and calculate them, respectively.

For $\tilde{O}_{e1}$, we further define and we can have the simplified form

$$\tilde{O}_{e1} = -g_s^2 \frac{1}{8\pi^{d/2}} \Gamma(d/2-1)(z_1^2)^{2-d/2} \int_0^1 dt_0 \int_0^1 d\eta (t_0)^{3-d} \psi_1^T((1-\eta t_0) z_1) \tilde{\Gamma} \psi_2(z_2)\psi_3(0), \tag{17}$$

with $t_0 = 1 - t_1$. The $t_0 \to 0$ corresponds to a UV divergence since that divergence is regularized by $d < 4$ and one end of the Wilson line approaches $z_1$ when $t_0 \to 0$. One can separate this divergence from the rest by using $\psi^T((1-\eta t_0)z_1) = (\psi^T((1-\eta t_0)z_1) - \psi^T(z_1)) + \psi^T(z_1)$. Then it is straightforward to obtain the results for these two parts

$$\tilde{O}_{e11} = \frac{\alpha_s C_F}{4\pi} \left( \frac{1}{\epsilon_{\rm UV}} + \log\left( \frac{1}{4}\mu^2 z_1^2 e^{2\gamma_E} \right) \right) \psi_1^T(z_1) \tilde{\Gamma} \psi_2(z_2)\psi_3(0), \tag{18}$$

$$\tilde{O}_{e12} = \frac{\alpha_s C_F}{2\pi} \int_0^1 d\eta \left( \frac{1-\eta}{\eta} \right)_+ \psi_1^T((1-\eta)z_1) \tilde{\Gamma} \psi_2(z_2)\psi_3(0). \tag{19}$$

The plus function is defined as $\int_0^1 du [G(u)]_+ F(u) = \int_0^1 du G(u)[F(u) - F(0)]$.

For $\tilde{O}_{e2}$, there is an IR divergence:

$$\tilde{O}_{e2} = -C_F \frac{g_s^2}{8\pi^2} \int_0^1 d\eta \left( \left( \ln\left( \frac{1}{4}\mu^2 z_1^2 e^{2\gamma_E} \right) + \frac{1}{\epsilon_{\rm IR}} + 2 \right) \left( \frac{1-\eta}{\eta} \right)_+ + \left( \frac{2\ln\eta}{\eta} \right)_+ \right) \psi_1^T(z_1(1-\eta)) \tilde{\Gamma} \psi_2(z_2)\psi_3(0). \tag{20}$$

Collecting all these pieces and removing the UV divergence in the $\overline{\rm MS}$ scheme give the final result:

$$\tilde{O}_e = \frac{\alpha_s C_F}{4\pi} \ln\left( \frac{1}{4}\mu_{\rm UV}^2 z_1^2 e^{2\gamma_E} \right) \psi_1^T(z_1) \Gamma \psi_2(z_2)\psi_3(0) - \frac{\alpha_s C_F}{\pi} \int_0^1 d\eta \left( \frac{\ln\eta}{\eta} \right)_+ \psi_1^T((1-\eta)z_1) \tilde{\Gamma} \psi_2(z_2)\psi_3(0) - \frac{\alpha_s C_F}{2\pi} \int_0^1 d\eta \left( \frac{1-\eta}{\eta} \right)_+ \left( \ln\left( \frac{1}{4}\mu_{\rm IR}^2 z_1^2 e^{2\gamma_E} \right) + \frac{1}{\epsilon_{\rm IR}} + 1 \right) \psi_1^T((1-\eta)z_1) \tilde{\Gamma} \psi_2(z_2)\psi_3(0), \tag{21}$$

where $\alpha_s = \frac{g_s^2}{4\pi}$. All the other cases will renormalized in this manner below without mention. Then, in the same manner, results for the quark-Wilson-line diagrams are derived as cases (e), (f), (h), and (i) all can be derived:

$$\begin{aligned}
\tilde{O}_e &= \frac{\alpha_s C_F}{4\pi} L_1^{\mathrm{UV}} \psi_1^T(z_1)\tilde{\Gamma}\psi_2(z_2)\psi_3(0) \\
&\quad -\frac{\alpha_s C_F}{2\pi}\int_0^1 d\eta \psi_1^T((1-\eta)z_1)\tilde{\Gamma}\psi_2(z_2)\psi_3(0)\left\{\left(L_1^{\mathrm{IR}}+1+\frac{1}{\epsilon_{\mathrm{IR}}}\right)\left(\frac{1-\eta}{\eta}\right)_+ + 2\left(\frac{\ln\eta}{\eta}\right)_+\right\}, \\
\tilde{O}_h &= \frac{\alpha_s C_F}{8\pi} L_1^{\mathrm{UV}} \psi_1^T(z_1)\tilde{\Gamma}\psi_2(z_2)\psi_3(0) \\
&\quad -\frac{\alpha_s C_F}{4\pi}\int_0^1 d\eta \psi_1^T(z_1)\tilde{\Gamma}\psi_2(z_2)\psi_3(\eta z_1)\left\{\left(L_1^{\mathrm{IR}}+1+\frac{1}{\epsilon_{\mathrm{IR}}}\right)\left(\frac{1-\eta}{\eta}\right)_+ + 2\left(\frac{\ln\eta}{\eta}\right)_+\right\}, \\
\tilde{O}_f &= \frac{\alpha_s C_F}{4\pi} L_2^{\mathrm{UV}} \psi_1^T(z_1)\tilde{\Gamma}\psi_2(z_2)\psi_3(0) \\
&\quad -\frac{\alpha_s C_F}{2\pi}\int_0^1 d\eta \psi_1^T(z_1)\tilde{\Gamma}\psi_2((1-\eta)z_2)\psi_3(0)\left\{\left(L_2^{\mathrm{IR}}+1+\frac{1}{\epsilon_{\mathrm{IR}}}\right)\left(\frac{1-\eta}{\eta}\right)_+ + 2\left(\frac{\ln\eta}{\eta}\right)_+\right\}, \\
\tilde{O}_i &= \frac{\alpha_s C_F}{8\pi} L_2^{\mathrm{UV}} \psi_1^T(z_1)\tilde{\Gamma}\psi_2(z_2)\psi_3(0) \\
&\quad -\frac{\alpha_s C_F}{4\pi}\int_0^1 d\eta \psi_1^T(z_1)\tilde{\Gamma}\psi_2(z_2)\psi_3(\eta z_2)\left\{\left(L_2^{\mathrm{IR}}+1+\frac{1}{\epsilon_{\mathrm{IR}}}\right)\left(\frac{1-\eta}{\eta}\right)_+ + 2\left(\frac{\ln\eta}{\eta}\right)_+\right\}.
\end{aligned} \tag{22}$$

Some abbreviations are used in the above:

$$L_1^{\mathrm{IR,UV}} = \ln\left(\frac{1}{4}\mu^2_{\mathrm{IR,UV}} z_1^2 e^{2\gamma_E}\right), \qquad L_2^{\mathrm{IR,UV}} = \ln\left(\frac{1}{4}\mu^2_{\mathrm{IR,UV}} z_2^2 e^{2\gamma_E}\right), \qquad L_{12}^{\mathrm{IR,UV}} = \ln\left(\frac{1}{4}\mu^2_{\mathrm{IR,UV}} (z_1-z_2)^2 e^{2\gamma_E}\right). \tag{23}$$

Since the color parameters for any chosen baryon out-states are fixed, we have preincluded these color parameters in the operator expressions to simplify the formulas.

### 2. Cases (d) and (g)

There are more subtleties in cases (d) and (g). We take case (d)

$$\tilde{O}_d = \psi_1(z_1)\left(ig\mu^{\frac{4-d}{2}}\int d^d\eta_1 \bar{\psi}_1(\eta_1)\not{A}(\eta_1)\psi_1(\eta_1)\right)\tilde{\Gamma}\left(-ig\mu^{\frac{4-d}{2}}\int_0^1 dt_1 z_2\cdot A(t_1 z_2)\right)\psi_2(z_2)\psi_3(0), \tag{24}$$

as a demonstration to illustrate them. Substituting and arranging as in the previous cases, the case (d) can be separated into two parts:

$$\tilde{O}_d = \tilde{O}_{d1} + \tilde{O}_{d2}, \tag{25}$$

$$\tilde{O}_{d1} = g^2\frac{(-i)^{d/2-1}}{8\pi^{d/2}}\mu^{4-d}\int d^dk_1\int_0^1 dt_1\int_0^1 d\beta_1\int_0^\infty d\sigma\sigma^{\frac{d}{2}-2}(-(z_1-t_1z_2)z_2) \tag{26}$$

$$\times e^{-i(k_1((\beta_1-1)z_1-\beta_1t_1z_2)+\sigma(z_1-t_1z_2)^2)}\psi_1^T(k_1)C\not{n}\gamma_5\psi_2(z_2)\psi_3(0), \tag{27}$$

$$\tilde{O}_{d2} = g^2\frac{(-i)^{d/2-1}}{8\pi^{d/2}}\mu^{4-d}\int d^dk_1\int_0^1 dt_1\int_0^1 d\beta_1\int_0^\infty d\sigma\sigma^{\frac{d}{2}-3}(\beta_1-1)(k_1\cdot z_2) \tag{28}$$

$$\times e^{-i(k_1((\beta_1-1)z_1-\beta_1t_1z_2)+\sigma(z_1-t_1z_2)^2)}\psi_1^T(k_1)C\not{n}\gamma_5\psi_2(z_2)\psi_3(0). \tag{29}$$

Through the calculation in the previous case, we now know that the IR and UV divergence have been separated during this operation.

For the $\tilde{O}_{d1}$, to make the inside two forms more explicitly, the range of the integral is split further as

$$\begin{aligned}\tilde{O}_{d1} &= \tilde{O}_{d11} - \tilde{O}_{d12},\\ &= g^2\frac{\Gamma(d/2-1)}{8\pi^{d/2}}\mu^{4-d}\left(\int_{\frac{z_1}{z_2}}^1 dt_1 - \int_{\frac{z_1}{z_2}}^0 dt_1\right)\int_0^1 d\beta_1(-(z_1-t_1z_2)z_2)((z_1-t_1z_2)^2)^{1-d/2}\\ &\quad\times\psi_1^T((1-\beta_1)z_1+\beta_1t_1z_2)C\not{n}\gamma_5\psi_2(z_2)\psi_3(0).\end{aligned} \tag{30}$$

Following that, we redefine the integral variables within them, respectively,

$$\begin{aligned}\tilde{O}_{d11} &= g^2\frac{\Gamma(d/2-1)}{8\pi^{d/2}}\frac{((z_1-z_2)^2)^{2-d/2}}{d-3}\mu^{4-d}\int_0^1 d\eta(\eta^{3-d}-1)\psi_1^T((1-\eta_1)z_1+\eta_1z_2)C\not{n}\gamma_5\psi_2(z_2)\psi_3(0),\\ \tilde{O}_{d12} &= g^2\frac{(z_1^2)^{2-d/2}}{d-3}\frac{\Gamma(d/2-1)}{8\pi^{d/2}}\mu^{4-d}\int_0^1 d\eta(\eta^{3-d}-1)\psi_1^T((1-\eta_1)z_1)(-C\not{n}\gamma_5)\psi_2(z_2)\psi_3(0).\end{aligned} \tag{31}$$

Now one can see that the two distinct forms of contributions have be separated.

For the $\tilde{O}_{d2}$, it can be divided into two parts:

$$\begin{aligned}\tilde{O}_{d2} &= \tilde{O}_{d21} - \tilde{O}_{d22},\\ \tilde{O}_{d21} &= \Gamma(d/2-2)g^2\frac{-1}{8\pi^{d/2}}\mu^{4-d}\int_0^1 d\beta_1\int_0^1 dt_1z_2(z_1-t_1z_2)^{-d+3}\psi_1^T((1-\beta_1)z_1+t_1\beta_1z_2)C\not{n}\gamma_5\psi_2(z_2)\psi_3(0),\\ \tilde{O}_{d22} &= -\Gamma(d/2-2)g^2\frac{-1}{8\pi^{d/2}}\mu^{4-d}\int d^dk_1\int_0^1 d\beta_1\int_0^1 dt_1z_2(z_1-t_1z_2)^{-d+3}e^{i(k_1\cdot z_1)}\psi_1^T(k_1)C\not{n}\gamma_5\psi_2(z_2)\psi_3(0).\end{aligned} \tag{32}$$

For $\tilde{O}_{d21}$, it can be further divided into two parts by splitting the range of the integral as before:

$$\begin{aligned}\tilde{O}_{d21} &= \tilde{O}_{d211} - \tilde{O}_{d212},\\ \tilde{O}_{d211} &= \Gamma(d/2-2)g^2\mu^{4-d}\frac{-1}{8\pi^{d/2}}\int_0^1 d\eta\int_{\frac{z_1-(z_1-z_2)\eta}{z_2}}^1 dt_1z_2(z_1-t_1z_2)^{-d+3}\frac{z_1-z_2}{z_1-t_1z_2}\psi_1^T((1-\eta)z_1+\eta_1z_2)C\not{n}\gamma_5\psi_2(z_2)\psi_3(0),\\ \tilde{O}_{d212} &= \Gamma(d/2-2)g^2\frac{-1}{8\pi^{d/2}}\mu^{4-d}\int_0^1 d\eta\int_{\frac{z_1}{z_2}}^0 dt_1z_2(z_1-t_1z_2)^{-d+3}\psi_1^T((1-\eta)z_1+t_1\eta z_2)C\not{n}\gamma_5\psi_2(z_2)\psi_3(0).\end{aligned} \tag{33}$$

After redefining the integral variables, above results can be computed as follows:

$$\begin{aligned}\tilde{O}_{d211} &= \Gamma(d/2-2)g^2\frac{-1}{8\pi^{d/2}}\mu^{4-d}((z_1-z_2)^2)^{\frac{4-d}{2}}\int_0^1 d\eta\frac{1-\eta^{3-d}}{d-3}\psi_1^T((1-\eta)z_1+\eta z_2)C\not{n}\gamma_5\psi_2(z_2)\psi_3(0),\\ \tilde{O}_{d212} &= -\Gamma(d/2-2)g^2\frac{-1}{8\pi^{d/2}}\mu^{4-d}(z_1^2)^{\frac{4-d}{2}}\int_0^1 d\eta\frac{(1-\eta^{3-d})}{d-3}\psi_1^T((1-\eta)z_1)(-C\not{n}\gamma_5)\psi_2(z_2)\psi_3(0).\end{aligned} \tag{34}$$

Next, we turn back to consider $\tilde{O}_{d22}$, which can be given directly

$$\tilde{O}_{d22} = -\mu^{4-d}\Gamma(d/2-2)g^2\frac{-1}{8\pi^{d/2}}\frac{((z_1-z_2)^2)^{2-d/2}-(z_1^2)^{2-d/2}}{d-4}\psi_1^T(z_1)C\not{n}\gamma_5\psi_2(z_2)\psi_3(0). \tag{35}$$

By summing all these pieces, one can obtain the $\tilde{O}_d$. Then, for the two cases in this pattern, we have the following:

$$\begin{aligned}\tilde{O}_d =& \frac{\alpha_s C_F}{8}(L_{12}^{\mathrm{UV}} - L_1^{\mathrm{UV}})\psi_1^T(z_1)\tilde{\Gamma}\psi_2(z_2)\psi_3(0)\\ &-\frac{\alpha_s C_F}{4\pi}\int_0^1 d\eta\psi_1^T((1-\eta)z_1+\eta z_2)\tilde{\Gamma}\psi_2(z_2)\psi_3(0)\left\{\left(L_{12}^{\mathrm{IR}}+1+\frac{1}{\epsilon_{\mathrm{IR}}}\right)\left(\frac{1-\eta}{\eta}\right)_+ + 2\left(\frac{\ln\eta}{\eta}\right)_+\right\}\\ &+\frac{\alpha_s C_F}{4\pi}\int_0^1 d\eta\psi_1^T((1-\eta)z_1)\tilde{\Gamma}\psi_2(z_2)\psi_3(0)\left\{\left(L_1^{\mathrm{IR}}+1+\frac{1}{\epsilon_{\mathrm{IR}}}\right)\left(\frac{1-\eta}{\eta}\right)_+ + 2\left(\frac{\ln\eta}{\eta}\right)_+\right\},\end{aligned} \tag{36}$$

$$\begin{aligned}\tilde{O}_g =& \frac{\alpha_s C_F}{8}(L_{12}^{\mathrm{UV}} - L_2^{\mathrm{UV}})\psi_1^T(z_1)\tilde{\Gamma}\psi_2(z_2)\psi_3(0)\\ &-\frac{\alpha_s C_F}{4\pi}\int_0^1 d\eta\psi_1^T(z_1)\tilde{\Gamma}\psi_2(\eta z_1+(1-\eta)z_2)\psi_2(z_2)\psi_3(0)\left\{\left(L_{12}^{\mathrm{IR}}+1+\frac{1}{\epsilon_{\mathrm{IR}}}\right)\left(\frac{1-\eta}{\eta}\right)_+ + 2\left(\frac{\ln\eta}{\eta}\right)_+\right\}\\ &+\frac{\alpha_s C_F}{4\pi}\int_0^1 d\eta\psi_1^T(z_1)\tilde{\Gamma}\psi_2((1-\eta)z_2)\psi_3(0)\left\{\left(L_2^{\mathrm{IR}}+1+\frac{1}{\epsilon_{\mathrm{IR}}}\right)\left(\frac{1-\eta}{\eta}\right)_+ + 2\left(\frac{\ln\eta}{\eta}\right)_+\right\}.\end{aligned} \tag{37}$$

There are no analogous terms in meson cases for these two cases. In fact, both of them are combinations of two forms. Specifically, there are certain terms in cases (d) and (g) that have the same form as cases (e) and (f), respectively. It is important to note that there are both IR and UV singularities in all these cases. The cases (e) and (f) differ from cases (d), (g), (h), and (i) in terms of their color coefficients, as detailed in [14]. More precisely, for cases (e), (f), (k), and (l), the color algebra yields the same results as in the meson case, represented by $C_F$. For cases (d) and (g), the color parameter is $-\frac{C_F}{2}$.

## B. q-q pattern

The quark-quark cases are presented in Figs. 1(a)–1(c). Since there are some differences between case (a) and cases (b) and (c), them deserve separate consideration.

### 1. Case (a)

In case (a), after performing the standard procedure, we have

$$\begin{aligned}\tilde{O}_a &= \tilde{O}_{a1} + \tilde{O}_{a2},\\ \tilde{O}_{a1} &= (d-2)g^2\mu^{4-d}\frac{(-i)^d}{16\pi^d}\int d^dk_1\int d^dk_2\int d^d\xi_2\frac{\sigma_1^{d/2-1}\sigma_2^{d/2-1}\sigma_3^{d/2-2}}{((\sigma_1+\sigma_3))^{d/2}}\frac{\sigma_1\sigma_2\sigma_3^2(-(z_1-z_2)^2)}{(\sigma_2\sigma_3+\sigma_1(\sigma_2+\sigma_3))^2}\\ &\quad\times e^{\frac{i(k_1^2\sigma_2+\sigma_1(4\sigma_2(k_1z_1+k_2z_2)+k_2^2)+\sigma_3((k_1+k_2)(k_1+k_2+4\sigma_1z_1)+4\sigma_2((k_1+k_2)z_2-\sigma_1(z_1-z_2)^2)))}{4\sigma_2\sigma_3+4\sigma_1(\sigma_2+\sigma_3)}-i(\sigma_2+\frac{\sigma_1\sigma_3}{\sigma_1+\sigma_3})\xi_2^2}\psi_1^T(k_1)C\not{n}\gamma^5\psi_2(k_2)\psi_3(0),\\ \tilde{O}_{a2} &= g^2\mu^{4-d}\frac{(-i)^d}{16\pi^d}\int d^dk_1\int d^dk_2\int d^d\xi_2\int d\sigma_1\int d\sigma_2\int d\sigma_3\frac{\sigma_1^{d/2-1}\sigma_2^{d/2-1}\sigma_3^{d/2-1}}{((\sigma_1+\sigma_3))^{d/2+1}}\\ &\quad\times e^{\frac{i(k_1^2\sigma_2+\sigma_1(4\sigma_2(k_1z_1+k_2z_2)+k_2^2)+\sigma_3((k_1+k_2)(k_1+k_2+4\sigma_1z_1)+4\sigma_2((k_1+k_2)z_2-\sigma_1(z_1-z_2)^2)))}{4\sigma_2\sigma_3+4\sigma_1(\sigma_2+\sigma_3)}-i(\sigma_2+\frac{\sigma_1\sigma_3}{\sigma_1+\sigma_3})\xi_2^2}\psi_1^T(k_1)C\gamma^\mu\not{\xi}_2\not{n}\gamma^5\not{\xi}_2\gamma_\mu\psi_2(k_2)\psi_3(0).\end{aligned} \tag{38}$$

The $\tilde{O}_{a1}$ and $\tilde{O}_{a2}$ can be simplified into

$$\begin{aligned}\tilde{O}_{a1} &= (d-2)g^2\mu^{4-d}\frac{1}{16\pi^{d/2}}\Gamma(d/2-1)\int_0^1 d\eta_1\int_0^1 d\eta_2((z_1-z_2)^2)^{2-d/2}\\ &\quad\times\psi_1^T((1-\eta_1)z_1+\eta_1z_2)(-C\not{n}\gamma^5)\psi_2((1-\eta_2)z_2+\eta_2z_1)\psi_3(0),\\ \tilde{O}_{a2} &= g^2\mu^{4-d}\frac{(D-2)^2}{2}\frac{1}{16\pi^{d/2}}\Gamma(-2+d/2)\int_0^1 d\eta_1\int_0^1 d\eta_2((z_1-z_2)^2)^{2-d/2}\\ &\quad\times\psi_1^T((1-\eta_1)z_1+\eta_1z_2)(-C\not{n}\gamma^5)\psi_2((1-\eta_2)z_2+\eta_2z_1)\psi_3(0).\end{aligned} \tag{39}$$

Getting them together:

$$\tilde{O}_a = -\frac{\alpha_s C_F}{4\pi}\int_0^1 d\eta_1 \int_0^{1-\eta_1} d\eta_2 \left(L_{12}^{\mathrm{IR}} - 3 + \frac{1}{\epsilon_{\mathrm{IR}}}\right)\psi_1^T(z_1(1-\eta_1)+z_2\eta_1)\tilde{\Gamma}\psi_2(z_2(1-\eta_2)+z_1\eta_2)\psi_3(0). \tag{40}$$

It is worth noting that when different projectors are chosen for the spatial correlator, only the results of the $\tilde{O}_{a1}$ term will be impacted. For example, if we switch the vector in $\tilde{\Gamma}$ from $n_z^\mu = (0,0,0,1)$ to $n_t^\mu = (1,0,0,0)$, the $\tilde{O}_{a1}$ term will acquire an additional negative sign.

### 2. Cases (b) and (c)

For case (b), after direct calculation, one reaches

$$\begin{aligned}\tilde{O}_b = {} & \frac{i(-i)^{3d/2-1}\mu^{4-d}g^2}{16\pi^d}\int d^dk_1\int d^dk_2\int d^d\xi_2\int_0^\infty d\sigma_1\int_0^\infty d\sigma_2\int_0^\infty d\sigma_3\frac{\sigma_1^{d/2-1}\sigma_2^{d/2-1}\sigma_3^{d/2-2}}{(-i(\sigma_1+\sigma_3))^{d/2}} \\ & \times e^{-i(\sigma_2+\frac{\sigma_1\sigma_3}{\sigma_1+\sigma_3})\xi_2^2+\frac{i(k_1^2\sigma_2+\sigma_1(4k_1\sigma_2z_1+k_2^2)+\sigma_3((k_1+k_2)(k_1+k_2+4\sigma_1z_1)-4\sigma_1\sigma_2z_1^2))}{4\sigma_2\sigma_3+4\sigma_1(\sigma_2+\sigma_3)}} \\ & \times \psi^T(k_1)C\gamma_\mu\left(\frac{-\not{k}_1 - 2\left(\sigma_3\left(\not{\xi}_2+\frac{\not{k}_2\sigma_1+\sigma_3(\not{k}_1+\not{k}_2+2\sigma_1\not{z}_1)}{2\sigma_2\sigma_3+2\sigma_1(\sigma_2+\sigma_3)}\right)+\sigma_1\not{z}_1\right)}{2(\sigma_1+\sigma_3)}+\not{z}_1\right)\not{n}_z\gamma_5\psi(z_2) \\ & \times\left(\not{\xi}_2+\frac{\not{k}_2\sigma_1+\sigma_3(\not{k}_1+\not{k}_2+2\sigma_1\not{z}_1)}{2\sigma_2\sigma_3+2\sigma_1(\sigma_2+\sigma_3)}\gamma^\mu\psi(k_2)\right),\end{aligned} \tag{41}$$

note that the bilinear part in it is proportional to $p^\mu$ in leading twist, then the spinor terms can be simplified vastly

$$\begin{aligned}\tilde{O}_b = {} & \frac{(-i)^d\mu^{4-d}g^2}{16\pi^d}\int d^dk_1\int d^dk_2\int d^d\xi_2\int_0^\infty d\sigma_1\int_0^\infty d\sigma_2\int_0^\infty d\sigma_3\frac{\sigma_1^{d/2-1}\sigma_2^{d/2-1}\sigma_3^{d/2-1}}{((\sigma_1+\sigma_3))^{d/2+1}} \\ & \times e^{-i(\sigma_2+\frac{\sigma_1\sigma_3}{\sigma_1+\sigma_3})\xi_2^2+\frac{i\sigma_1z_1(k_1\sigma_2+\sigma_3(k_1+k_2-\sigma_2z_1))}{\sigma_2\sigma_3+\sigma_1(\sigma_2+\sigma_3)}}\psi^T(k_1)C\gamma_\mu\not{\xi}_2\not{n}_z\gamma_5\psi(z_2)(\not{\xi}_2\gamma^\mu\psi(k_2)).\end{aligned} \tag{42}$$

Then it can be simplified to

$$\tilde{O}_b = (1-2/d)\frac{d\mu^{4-d}g^2\Gamma(d/2-2)}{32\pi^{d/2}}(z_1^2)^{2-d/2}\int_0^1 d\eta_1\int_0^1 d\eta_2\psi^T((1-\eta_1)z_1)(-C\not{n}_z\gamma_5)\psi(z_2)\psi(\eta_2z_1). \tag{43}$$

Following the same routine, all results within this pattern can be written down directly

$$\tilde{O}_b = -\frac{\alpha_s C_F}{8\pi}\int_0^1 d\eta_1\int_0^{1-\eta_1} d\eta_2\left(L_1^{\mathrm{IR}} - 1 + \frac{1}{\epsilon_{\mathrm{IR}}}\right)\psi_1^T((1-\eta_1)z_1)\tilde{\Gamma}\psi_2(z_2)\psi_3(\eta_2z_1), \tag{44}$$

$$\tilde{O}_c = -\frac{\alpha_s C_F}{8\pi}\int_0^1 d\eta_1\int_0^{1-\eta_1} d\eta_2\left(L_2^{\mathrm{IR}} - 1 + \frac{1}{\epsilon_{\mathrm{IR}}}\right)\psi_1^T(z_1)\tilde{\Gamma}\psi_2((1-\eta_1)z_2)\psi_3(\eta_2z_2). \tag{45}$$

It should be noted that case (a) possesses an additional finite component in comparison to cases (b) and (c). From the calculations presented above, it becomes evident that this difference arises from an extra component in case (a). Notably, there are no terms analogous to those in case (a) in the meson LCDAs calculation. Additionally, there is no UV divergence in all these operators.

## C. W-W pattern

Last but not least, the W-W pattern, corresponding to Figs. 1(j)–1(l) will be considered. After the aforementioned preparation, the corresponding one-loop results can be easily obtained:

$$\tilde{O}_k = \frac{\alpha_s C_F}{2\pi}(L_1^{\mathrm{UV}} + 2)\psi_1^T(z_1)\tilde{\Gamma}\psi_2(z_2)\psi_3(0), \tag{46}$$

$$\tilde{O}_l = \frac{\alpha_s C_F}{2\pi}(L_2^{\mathrm{UV}} + 2)\psi_1^T(z_1)\tilde{\Gamma}\psi_2(z_2)\psi_3(0), \tag{47}$$

$$\tilde{O}_j = -\frac{\alpha_s C_F}{4\pi}(L_1^{\mathrm{UV}} + L_2^{\mathrm{UV}} - L_{12}^{\mathrm{UV}} + 2)\psi_1^T(z_1)\tilde{\Gamma}\psi_2(z_2)\psi_3(0). \tag{48}$$

Note that in these cases, only UV divergences arise when the two ends of the gluons coincide with each other.

### D. One-loop results for spatial correlator

The final results for the spatial correlator to one-loop order are given as

$$\begin{aligned}
M(\nu_1,\nu_2,0,z^2,\mu) = &\left\{1+\frac{\alpha_s C_F}{\pi}\left(\frac{1}{2}L_1^{\mathrm{UV}}+\frac{1}{2}L_2^{\mathrm{UV}}+\frac{1}{2}L_{12}^{\mathrm{UV}}+\frac{3}{2}\right)\right\}M_0(\nu_1,\nu_2,0,z^2,\mu)\\
&-\frac{\alpha_s C_F}{8\pi}\int_0^1 d\eta_1\int_0^{1-\eta_1} d\eta_2\left\{2\left(L_{12}^{\mathrm{IR}}-3+\frac{1}{\epsilon_{\mathrm{IR}}}\right)M_0((1-\eta_1)\nu_1+\eta_1\nu_2,(1-\eta_2)\nu_2+\eta_2\nu_1,0,z^2,\mu)\right.\\
&\left.+\left(L_1^{\mathrm{IR}}-1+\frac{1}{\epsilon_{\mathrm{IR}}}\right)M_0((1-\eta_1)\nu_1,\nu_2,\eta_2\nu_1,z^2,\mu)+\left(L_2^{\mathrm{IR}}-1+\frac{1}{\epsilon_{\mathrm{IR}}}\right)M_0(\nu_1,(1-\eta_1)\nu_2,\eta_2\nu_2,z^2,\mu)\right\}\\
&-\frac{\alpha_s C_F}{4\pi}\int_0^1 d\eta\left\{(M_0((1-\eta)z_1,z_2,0,P^z,\mu)+M_0(z_1,z_2,\eta z_1,P^z,\mu))\left\{\left(L_1^{\mathrm{IR}}+1+\frac{1}{\epsilon_{\mathrm{IR}}}\right)\left(\frac{1-\eta}{\eta}\right)_+\right.\right.\\
&\left.\left.+2\left(\frac{\ln\eta}{\eta}\right)_+\right\}+(M_0(z_1,(1-\eta)z_2,0,P^z,\mu)+M_0(z_1,z_2,\eta z_2,P^z,\mu))\left\{\left(L_2^{\mathrm{IR}}+1+\frac{1}{\epsilon_{\mathrm{IR}}}\right)\left(\frac{1-\eta}{\eta}\right)_+\right.\right.\\
&\left.\left.+2\left(\frac{\ln\eta}{\eta}\right)_+\right\}+(M_0((1-\eta)\nu_1+\eta\nu_2,\nu_2,0,z^2,\mu)+M_0(z_1,(1-\eta)z_2+\eta z_1,0,P^z,\mu))\right.\\
&\left.\times\left\{\left(L_{12}^{\mathrm{IR}}+1+\frac{1}{\epsilon_{\mathrm{IR}}}\right)\left(\frac{1-\eta}{\eta}\right)_+ +2\left(\frac{\ln\eta}{\eta}\right)_+\right\}\right\},
\end{aligned} \tag{49}$$

where $M_0$ stands for tree-level matrix element. We have checked that these results are consistent with the calculation in the momentum space [14]. Moreover, one can see the UV and IR behaviors clearly in the coordinate space, which is convenient for the renormalization scheme to be established below.

### E. Light cone correlator

To obtain the light cone results, one just needs to perform a similar calculation as the equal-time correlator case, up to choose $z^2 = 0$ and $\Gamma = C\gamma_5 \not{n}$. The light cone results can be written down straightforwardly as a byproduct. Besides, they will be used for matching later. Hence these light cone results will be outlined. It is important to note that three cases corresponding to the self-energy of Wilson lines do not contribute to the light cone case. For the q-q pattern:

$$\begin{aligned}
O_a &= -\frac{\alpha_s C_F}{4\pi}\frac{1}{\epsilon_{\mathrm{IR}}}\int_0^1 d\eta_1\int_0^{1-\eta_1} d\eta_2\psi_1^T(z_1(1-\eta_1)+z_2\eta_1)\Gamma\psi_2(z_2(1-\eta_2)+z_1\eta_2)\psi_2(0),\\
O_b &= -\frac{\alpha_s C_F}{8\pi}\frac{1}{\epsilon_{\mathrm{IR}}}\int_0^1 d\eta_1\int_0^{1-\eta_1} d\eta_2\psi_1^T((1-\eta_1)z_1)\Gamma\psi_2(z_2)\psi_3(\eta_2 z_1),\\
O_c &= -\frac{\alpha_s C_F}{8\pi}\frac{1}{\epsilon_{\mathrm{IR}}}\int_0^1 d\eta_1\int_0^{1-\eta_1} d\eta_2\psi_1^T(z_1)\Gamma\psi_2((1-\eta_1)z_2)\psi_3(\eta_2 z_2).
\end{aligned} \tag{50}$$

For the q-W pattern:

$$
\begin{aligned}
O_e &= -\frac{\alpha_s C_F}{2\pi}\frac{1}{\epsilon_{\mathrm{IR}}}\int_0^1 d\eta\left(\frac{1-\eta}{\eta}\right)_+ \psi_1^T((1-\eta)z_1)\Gamma\psi_2(z_2)\psi_3(0),\\
O_h &= -\frac{\alpha_s C_F}{4\pi}\frac{1}{\epsilon_{\mathrm{IR}}}\int_0^1 d\eta\left(\frac{1-\eta}{\eta}\right)_+ \psi_1^T(z_1)\Gamma\psi_2(z_2)\psi_3(\eta z_1),\\
O_f &= -\frac{\alpha_s C_F}{2\pi}\frac{1}{\epsilon_{\mathrm{IR}}}\int_0^1 d\eta\left(\frac{1-\eta}{\eta}\right)_+ \psi_1^T(z_1)\Gamma\psi_2((1-\eta)z_2)\psi_3(0),\\
O_i &= -\frac{\alpha_s C_F}{4\pi}\frac{1}{\epsilon_{\mathrm{IR}}}\int_0^1 d\eta\left(\frac{1-\eta}{\eta}\right)_+ \psi_1^T(z_1)\Gamma\psi_2(z_2)\psi_3(\eta z_2),\\
O_d &= -\frac{\alpha_s C_F}{4\pi}\frac{1}{\epsilon_{\mathrm{IR}}}\int_0^1 d\eta\left(\frac{1-\eta}{\eta}\right)_+ (\psi_1^T((1-\eta)z_1+\eta z_2)\Gamma\psi_2(z_2)\psi_3(0)-\psi_1^T((1-\eta)z_1)\Gamma\psi_2(z_2)\psi_3(0)),\\
O_g &= -\frac{\alpha_s C_F}{4\pi}\frac{1}{\epsilon_{\mathrm{IR}}}\int_0^1 d\eta\left(\frac{1-\eta}{\eta}\right)_+ (\psi_1^T(z_1)\Gamma\psi_2(\eta z_1+(1-\eta)z_2)\psi_3(0)-\psi_1^T(z_1)\Gamma\psi_2((1-\eta)z_2)\psi_3(0)).
\end{aligned}
\tag{51}
$$

Collecting them together, we have

$$
\begin{aligned}
\mathcal{I}(\nu_1,\nu_2,0,\mu) = \mathcal{I}_0(\nu_1,\nu_2,0,\mu) &- \frac{\alpha_s C_F}{8\pi}\frac{1}{\epsilon_{\mathrm{IR}}}\Bigg\{2\int_0^1 d\eta_1\int_0^{1-\eta_1} d\eta_2[\mathcal{I}_0((1-\eta_1)\nu_1+\eta_1\nu_2,(1-\eta_2)\nu_2+\eta_2\nu_1,0,\mu)\\
&+\mathcal{I}_0((1-\eta_1)\nu_1,\nu_2,\eta_2\nu_1,\mu)+\mathcal{I}_0(z_1,(1-\eta_1)\nu_2,\eta_2\nu_2,\mu)]\\
&+2\int_0^1 d\eta\left(\frac{1-\eta}{\eta}\right)_+\{(\mathcal{I}_0((1-\eta)\nu_1+\eta\nu_2,\nu_2,0,\mu)+\mathcal{I}_0(\nu_1,(1-\eta)\nu_2+\eta\nu_1,0,\mu))\\
&+(\mathcal{I}_0((1-\eta)\nu_1,\nu_2,0,\mu)+\mathcal{I}_0(\nu_1,\nu_2,\eta\nu_1,\mu))+(\mathcal{I}_0(\nu_1,(1-\eta)\nu_2,0,\mu)+\mathcal{I}_0(\nu_1,\nu_2,\eta\nu_2,\mu))\}\Bigg\}.
\end{aligned}
\tag{52}
$$

The light cone correlator can be normalized by dividing it by its 0-momentum matrix element

$$
\mathfrak{I}(\nu_1,\nu_2,\nu_3,\mu)\equiv\frac{\mathcal{I}(\nu_1,\nu_2,\nu_3,\mu)}{\mathcal{I}(0,0,0,\mu)}. \tag{53}
$$

## IV. RATIO SCHEME IN SMALL SPATIAL SEPARATION

### A. Renormalization and reduced ITD

In the subsequent sections, all UV divergences will be addressed using the widely adopted ratio scheme. Fundamentally, the validity of the ratio scheme relies on the principle of multiplicative renormalization for composite operators. When UV renormalization parameters can be factorized out, it becomes feasible to provide a ratio-form definition of the distribution

$$
\mathfrak{M}(\nu_1,\nu_2,\nu_3,z^2)=\left.\frac{M(\nu_1,\nu_2,\nu_3,z^2,\mu)}{M(\omega\nu_1,\omega\nu_2,\omega\nu_3,z^2,\mu)}\right|_{\omega=0} \tag{54}
$$

to cancel UV divergence out. Based on the one-loop results, it is evident that the ratio scheme will not affect the existing IR physics. Additionally, this scheme efficiently eliminates the lattice discreteness effect over short distances. Under this scheme, the results of the spatial correlator can be readily converted to

$$\begin{aligned}\mathfrak{M}(\nu_1,\nu_2,0,z^2) &= \mathfrak{M}_0(\nu_1,\nu_2,0,z^2) - \frac{\alpha_s C_F}{8\pi}\int_0^1 d\eta_1 \int_0^{1-\eta_1} d\eta_2 \\ &\times \left\{ \left(L_1^{\rm IR} - 1 + \frac{1}{\epsilon_{\rm IR}}\right)(\mathfrak{M}_0((1-\eta_1)\nu_1,\nu_2,\eta_2\nu_1,z^2) - \mathfrak{M}_0(\nu_1,\nu_2,0,z^2)) \right. \\ &+ \left(L_2^{\rm IR} - 1 + \frac{1}{\epsilon_{\rm IR}}\right)(\mathfrak{M}_0(\nu_1,(1-\eta_1)\nu_2,\eta_2\nu_2,z^2) - \mathfrak{M}_0(\nu_1,\nu_2,0,z^2)) \\ &\left. + 2\left(L_{12}^{\rm IR} - 3 + \frac{1}{\epsilon_{\rm IR}}\right)(\mathfrak{M}_0((1-\eta_1)\nu_1+\eta_1\nu_2,(1-\eta_2)\nu_2+\eta_2\nu_1,0,z^2) - \mathfrak{M}_0(\nu_1,\nu_2,0,z^2)) \right\} \\ &- \frac{\alpha_s C_F}{4\pi}\int_0^1 d\eta \left\{ (\mathfrak{M}_0(\nu_1,(1-\eta)\nu_2,0,z^2) + \mathfrak{M}_0(\nu_1,\nu_2,\eta\nu_2,z^2)) \left\{ \left(L_2^{\rm IR} + 1 + \frac{1}{\epsilon_{\rm IR}}\right)\left(\frac{1-\eta}{\eta}\right)_+ + 2\left(\frac{\ln\eta}{\eta}\right)_+ \right\} \right. \\ &+ (\mathfrak{M}_0((1-\eta)\nu_1,\nu_2,0,z^2) + \mathfrak{M}_0(\nu_1,\nu_2,\eta\nu_1,z^2)) \left\{ \left(L_1^{\rm IR} + 1 + \frac{1}{\epsilon_{\rm IR}}\right)\left(\frac{1-\eta}{\eta}\right)_+ + 2\left(\frac{\ln\eta}{\eta}\right)_+ \right\} \\ &\left. + (\mathfrak{M}_0((1-\eta)\nu_1+\eta\nu_2,\nu_2,0,z^2) + \mathfrak{M}_0(\nu_1,(1-\eta)\nu_2+\eta\nu_1,0,z^2)) \right. \\ &\left. \times \left\{ \left(L_{12}^{\rm IR} + 1 + \frac{1}{\epsilon_{\rm IR}}\right)\left(\frac{1-\eta}{\eta}\right)_+ + 2\left(\frac{\ln\eta}{\eta}\right)_+ \right\} \right\}. \end{aligned} \tag{55}$$

It should be mentioned that the validity of multiplicative renormalization has not been proved. General proof to all orders is still required. Furthermore, it can be verified through lattice computations, which will help clarify the range of its validity.

### B. Matching and RGE

Although the light cone correlator and spatial correlator are both ITD with different coordinate choices. But one cannot simply turn the spatial correlator to the light cone correlator by approaching the $z^2$ to zero due to the divergences.

The connection between equal-time and light cone physics can be established through a matching process:

$$\mathfrak{M}(\nu_1,\nu_2,0,z^2) = \int_0^1 \mathrm{d}\eta_1 \int_0^{1-\eta_1} \mathrm{d}\eta_2 \tag{56}$$

$$\times C(\eta_1,\eta_2,\nu_1,\nu_2,\mu)\mathcal{I}(\eta_1,\eta_2,\nu_1,\nu_2,\mu) + \mathcal{O}(z^2), \tag{57}$$

where $C(\eta_1,\eta_2,\nu_1,\nu_2,\mu)$ stands for the matching kernel. It should be mentioned that due to the complex nature of the dependence on $\eta_i$s and $\nu_i$s, we present the arguments in a nonstandard form within $\mathcal{I}$.

Combining Eqs. (52) and (55), we have

$$\begin{aligned}\mathfrak{M}(\nu_1,\nu_2,0,z_i^2) &= \mathfrak{F}(\nu_1,\nu_2,0,\mu) - \frac{\alpha_s C_F}{8\pi}\int_0^1 d\eta_1 \int_0^{1-\eta_1} d\eta_2 \\ &\times \{(L_1^{\rm UV}-1)\mathfrak{F}((1-\eta_1)\nu_1,\nu_2,\eta_2\nu_1,\mu) + (L_2^{\rm UV}-1)\mathfrak{F}(\nu_1,(1-\eta_1)\nu_2,\eta_2\nu_2,\mu) \\ &+ 2(L_{12}^{\rm UV}-3)\mathfrak{F}((1-\eta_1)\nu_1+\eta_1\nu_2,(1-\eta_2)\nu_2+\eta_2\nu_1,0,\mu) \\ &- (L_1^{\rm UV}-1)\mathfrak{F}(\nu_1,\nu_2,0,\mu) - (L_2^{\rm UV}-1)\mathfrak{F}(\nu_1,\nu_2,0,\mu) - 2(L_{12}^{\rm UV}-3)\mathfrak{F}(\nu_1,\nu_2,0,\mu)\} \\ &- \frac{\alpha_s C_F}{4\pi}\int_0^1 d\eta \left\{ (\mathfrak{F}((1-\eta)\nu_1,\nu_2,0,\mu) + \mathfrak{F}(\nu_1,\nu_2,\eta\nu_1,\mu)) \left\{ (L_1^{\rm UV}+1)\left(\frac{1-\eta}{\eta}\right)_+ + 2\left(\frac{\ln\eta}{\eta}\right)_+ \right\} \right. \\ &+ (\mathfrak{F}(\nu_1,(1-\eta)\nu_2,0,\mu) + \mathfrak{F}(\nu_1,\nu_2,\eta\nu_2,\mu)) \left\{ (L_2^{\rm UV}+1)\left(\frac{1-\eta}{\eta}\right)_+ + 2\left(\frac{\ln\eta}{\eta}\right)_+ \right\} \\ &\left. + (\mathfrak{F}(\nu_1,(1-\eta)\nu_2+\eta\nu_1,0,\mu) + \mathfrak{F}(\nu_1,(1-\eta)\nu_2+\eta\nu_1,0,\mu)) \left\{ (L_{12}^{\rm UV}+1)\left(\frac{1-\eta}{\eta}\right)_+ + 2\left(\frac{\ln\eta}{\eta}\right)_+ \right\} \right\}. \end{aligned} \tag{58}$$

As expect, the IR structures within the light cone operator and spatial correlator are identical and cancel each other out in the calculation. Once have extracted the light cone correlator from the spatial correlator using Eq. (58),

one can immediately obtain the LCDAs through performing Fourier transformation. However, given that the ratio scheme is merely valid in the perturbative region, other methods need to be invoked in other regions. In regions beyond the perturbative region, it is possible to utilize various models or engage in direct global fitting procedures. For example, in paper [15], the long-distance physics are addressed by the self-renormalization.

Moreover, the evolution equation can be derived. By following the standard procedure for constructing RGEs, one can deduce

$$\begin{aligned}\mu\frac{\partial}{\partial\mu}\mathfrak{F}(\nu_1,\nu_2,0,\mu) &= \frac{\alpha_s C_F}{4\pi}\int_0^1 d\eta_1\int_0^{1-\eta_1} d\eta_2\{2\mathfrak{F}((1-\eta_1)\nu_1+\eta_1\nu_2,(1-\eta_2)\nu_2+\eta_2\nu_1,0,\mu)-2\mathfrak{F}(\nu_1,\nu_2,0,\mu)\\ &+\mathfrak{F}((1-\eta_1)\nu_1,\nu_2,\eta_2\nu_1,\mu)-\mathfrak{F}(\nu_1,\nu_2,0,\mu)+\mathfrak{F}(\nu_1,(1-\eta_1)\nu_2,\eta_2\nu_2,\mu)-\mathfrak{F}(\nu_1,\nu_2,0,\mu)\}\\ &+\frac{\alpha_s C_F}{2\pi}\int_0^1 d\eta\left(\frac{1-\eta}{\eta}\right)_+\{\mathfrak{F}((1-\eta)\nu_1+\eta\nu_2,\nu_2,0,\mu)+\mathfrak{F}(\nu_1,(1-\eta)\nu_2+\eta\nu_1,0,\mu)\\ &+\mathfrak{F}((1-\eta)\nu_1,\nu_2,0,\mu)+\mathfrak{F}(\nu_1,(1-\eta)\nu_2,0,\mu)+\mathfrak{F}(\nu_1,\nu_2,\eta\nu_1,\mu)+\mathfrak{F}(\nu_1,\nu_2,\eta\nu_2,\mu)\},\end{aligned}\tag{59}$$

which is consistent with the discussions made in paper [8]. It is worth noting that unlike the cases of meson DAs or PDFs, where the RGE can be obtained by taking derivatives with respect to $\ln z^2$. This can be substantiated by the following considerations. For meson DAs or PDFs, there are only one variables need to be consider, the $\ln z^2$ used for taking derivative is clear. While in the baryon case, there are three distinct $\ln z^2$ dependencies, namely $\ln z_1^2$, $\ln z_2^2$, and $\ln(z_1-z_2)^2$, need to be considered, which makes it hard to perform the derivative. Even if we were to focus on derivatives involving just one of the $\ln z^2$, it remains difficult to obtain a kernel-like result in a concise form. In meson cases, the use of translation invariance allows for a shift in the dependence on integral variables, resulting in a more compact expression. In the baryon case, the translation invariance extends to three fields. When trying to perform a shift operation similar to what is done in meson cases, it always includes an additional quark. This makes it challenging to express the results in a more concise manner. Therefore, the equivalence between the RGE and derivatives with respect to $\ln z^2$ of the spatial correlator are not explicit in this context.

## V. SUMMARY

To obtain the light baryon LCDAs through lattice QCD using spatial correlation, we have calculated the spatial correlator to one-loop order. And we have conducted a comprehensive analysis of their UV and IR properties. Subsequently, we applied renormalization via the ratio scheme. The renormalized spatial correlator has been related to the light baryon correlator through matching. This allows for the direct extraction of the light-baryon light cone correlator. These results provide a fundamental methodology for extracting the baryon LCDA from first principles. The validation of the ratio renormalization scheme for the light baryons is based on the multiplicative renormalization, which still need a robust proof in the future studies. The efficiency and utility of the adopted ratio scheme have been demonstrated, offering a practical approach to investigate the light baryon LCDA on the lattice. This procedure can also be extended for the examination of other light cone physical quantities of light baryons in collaboration with lattice QCD in future research endeavors.

## ACKNOWLEDGMENTS

We would like to thank Wei Wang, Yushan Su, Jun Zeng, and Zhifu Deng for their insightful comments and invaluable discussions. This work is supported in part by the Natural Science Foundation of China under Grants No. 12125503, No. U2032102, No. 12061131006, and No. 12335003.

[1] H.-H. Shih, S.-C. Lee, and H.-n. Li, The $\Lambda_b \to p$ lepton anti-neutrino decay in perturbative QCD, Phys. Rev. D **59**, 094014 (1999).

[2] LHCb Collaboration, Determination of the quark coupling strength $|V_{ub}|$ using baryonic decays, Nat. Phys. **11**, 743 (2015).

[3] J. A. Bailey *et al.* (Fermilab Lattice, MILC Collaborations), $B \to \pi \ell \ell$ form factors for new-physics searches from lattice QCD, Phys. Rev. Lett. **115**, 152002 (2015).

[4] R. Aaij *et al.* (LHCb Collaboration), Differential branching fraction and angular analysis of $\Lambda_b^0 \to \Lambda \mu^+ \mu^-$ decays, J. High Energy Phys. 06 (2015) 115; 09 (2018) 145(E).

[5] R. Aaij *et al.* (LHCb Collaboration), Measurement of the photon polarization in $\Lambda_b^0 \to \Lambda \gamma$ decays, Phys. Rev. D **105**, L051104 (2022).

[6] V. L. Chernyak and I. R. Zhitnitsky, Nucleon wave function and nucleon form-factors in QCD, Nucl. Phys. **B246**, 52 (1984).

[7] I. D. King and C. T. Sachrajda, Nucleon wave functions and QCD sum rules, Nucl. Phys. **B279**, 785 (1987).

[8] V. M. Braun, S. E. Derkachov, G. P. Korchemsky, and A. N. Manashov, Baryon distribution amplitudes in QCD, Nucl. Phys. **B553**, 355 (1999).

[9] I. V. Anikin, V. M. Braun, and N. Offen, Nucleon form factors and distribution amplitudes in QCD, Phys. Rev. D **88**, 114021 (2013).

[10] M. Gockeler *et al.*, Nucleon distribution amplitudes from lattice QCD, Phys. Rev. Lett. **101**, 112002 (2008).

[11] V. M. Braun *et al.* (QCDSF Collaboration), Nucleon distribution amplitudes and proton decay matrix elements on the lattice, Phys. Rev. D **79**, 034504 (2009).

[12] G. S. Bali *et al.*, Light-cone distribution amplitudes of the baryon octet, J. High Energy Phys. 02 (2016) 070.

[13] G. S. Bali *et al.* (RQCD Collaboration), Light-cone distribution amplitudes of octet baryons from lattice QCD, Eur. Phys. J. A **55**, 116 (2019).

[14] Z.-F. Deng, C. Han, W. Wang, J. Zeng, and J.-L. Zhang, Light-cone distribution amplitudes of a light baryon in large-momentum effective theory, J. High Energy Phys. 07 (2023) 191.

[15] C. Han, Y. Su, W. Wang, and J.-L. Zhang, Hybrid renormalization for quasi distribution amplitudes of a light baryon, J. High Energy Phys. 12 (2023) 044.

[16] X. Ji, Parton physics from large-momentum effective field theory, Sci. China Phys. Mech. Astron. **57**, 1407 (2014).

[17] X. Ji, J.-H. Zhang, and Y. Zhao, More on large-momentum effective theory approach to parton physics, Nucl. Phys. **B924**, 366 (2017).

[18] X. Ji, Y.-S. Liu, Y. Liu, J.-H. Zhang, and Y. Zhao, Large-momentum effective theory, Rev. Mod. Phys. **93**, 035005 (2021).

[19] X. Ji, Why is LaMET an effective field theory for partonic structure?, arXiv:2007.06613.

[20] X. Ji, Parton physics on a Euclidean lattice, Phys. Rev. Lett. **110**, 262002 (2013).

[21] X. Xiong, X. Ji, J.-H. Zhang, and Y. Zhao, One-loop matching for parton distributions: Nonsinglet case, Phys. Rev. D **90**, 014051 (2014).

[22] J.-W. Chen, S. D. Cohen, X. Ji, H.-W. Lin, and J.-H. Zhang, Nucleon helicity and transversity parton distributions from lattice QCD, Nucl. Phys. **B911**, 246 (2016).

[23] X. Xiong, T. Luu, and U.-G. Meißner, Quasi-parton distribution function in lattice perturbation theory, arXiv:1705.00246.

[24] W. Wang, S. Zhao, and R. Zhu, Gluon quasidistribution function at one loop, Eur. Phys. J. C **78**, 147 (2018).

[25] J.-W. Chen, T. Ishikawa, L. Jin, H.-W. Lin, Y.-B. Yang, J.-H. Zhang, and Y. Zhao, Parton distribution function with nonperturbative renormalization from lattice QCD, Phys. Rev. D **97**, 014505 (2018).

[26] Y.-S. Liu, J.-W. Chen, L. Jin, R. Li, H.-W. Lin, Y.-B. Yang, J.-H. Zhang, and Y. Zhao, Nucleon transversity distribution at the physical pion mass from lattice QCD, arXiv:1810.05043.

[27] Z.-Y. Fan, Y.-B. Yang, A. Anthony, H.-W. Lin, and K.-F. Liu, Gluon quasi-parton-distribution functions from lattice QCD, Phys. Rev. Lett. **121**, 242001 (2018).

[28] M. A. Ebert, I. W. Stewart, and Y. Zhao, Determining the nonperturbative Collins-Soper kernel from lattice QCD, Phys. Rev. D **99**, 034505 (2019).

[29] J.-H. Zhang, X. Ji, A. Schäfer, W. Wang, and S. Zhao, Accessing gluon parton distributions in large momentum effective theory, Phys. Rev. Lett. **122**, 142001 (2019).

[30] Y.-S. Liu *et al.*, Unpolarized isovector quark distribution function from lattice QCD: A systematic analysis of renormalization and matching, Phys. Rev. D **101**, 034020 (2020).

[31] J.-W. Chen, L. Jin, H.-W. Lin, Y.-S. Liu, Y.-B. Yang, J.-H. Zhang, and Y. Zhao, Lattice calculation of parton distribution function from LaMET at physical pion mass with large nucleon momentum, arXiv:1803.04393.

[32] J.-H. Zhang, J.-W. Chen, L. Jin, H.-W. Lin, A. Schäfer, and Y. Zhao, First direct lattice-QCD calculation of the x-dependence of the pion parton distribution function, Phys. Rev. D **100**, 034505 (2019).

[33] Y. Chai *et al.*, Parton distribution functions of $\Delta^+$ on the lattice, Proc. Sci. LATTICE2019 (**2019**) 270 [arXiv:1907.09827].

[34] K. Cichy, L. Del Debbio, and T. Giani, Parton distributions from lattice data: The nonsinglet case, J. High Energy Phys. 10 (2019) 137.

[35] T. Izubuchi, L. Jin, C. Kallidonis, N. Karthik, S. Mukherjee, P. Petreczky, C. Shugert, and S. Syritsyn, Valence parton distribution function of pion from fine lattice, Phys. Rev. D **100**, 034516 (2019).

[36] W. Wang, J.-H. Zhang, S. Zhao, and R. Zhu, Complete matching for quasidistribution functions in large momentum effective theory, Phys. Rev. D **100**, 074509 (2019).

[37] S. Bhattacharya, K. Cichy, M. Constantinou, A. Metz, A. Scapellato, and F. Steffens, The role of zero-mode contributions in the matching for the twist-3 PDFs $e(x)$ and $h_L(x)$, Phys. Rev. D **102**, 114025 (2020).

[38] S. Bhattacharya, K. Cichy, M. Constantinou, A. Metz, A. Scapellato, and F. Steffens, Insights on proton structure from lattice QCD: The twist-3 parton distribution function $g_T(x)$, Phys. Rev. D **102**, 111501 (2020).

[39] Y. Chai *et al.*, Parton distribution functions of $\Delta^+$ on the lattice, Phys. Rev. D **102**, 014508 (2020).
[40] C. Shugert, X. Gao, T. Izubichi, L. Jin, C. Kallidonis, N. Karthik, S. Mukherjee, P. Petreczky, S. Syritsyn, and Y. Zhao, Pion valence quark PDF from lattice QCD, in *37th International Symposium on Lattice Field Theory* (2020), arXiv:2001.11650.
[41] H.-W. Lin, J.-W. Chen, Z. Fan, J.-H. Zhang, and R. Zhang, Valence-quark distribution of the kaon and pion from lattice QCD, Phys. Rev. D **103**, 014516 (2021).
[42] C. Alexandrou, K. Cichy, M. Constantinou, J. R. Green, K. Hadjiyiannakou, K. Jansen, F. Manigrasso, A. Scapellato, and F. Steffens, Lattice continuum-limit study of nucleon quasi-PDFs, Phys. Rev. D **103**, 094512 (2021).
[43] S. Bhattacharya, K. Cichy, M. Constantinou, A. Metz, A. Scapellato, and F. Steffens, Parton distribution functions beyond leading twist from lattice QCD: The $h_L(x)$ case, Phys. Rev. D **104**, 114510 (2021).
[44] S. Bhattacharya, K. Cichy, M. Constantinou, A. Metz, A. Scapellato, and F. Steffens, Twist-3 partonic distributions from lattice QCD, SciPost Phys. Proc. **8**, 057 (2022).
[45] F. Yao *et al.* (Lattice Parton Collaboration), Nucleon transversity distribution in the continuum and physical mass limit from lattice QCD, Phys. Rev. Lett. **131**, 261901 (2023).
[46] R. Zhang, J. Holligan, X. Ji, and Y. Su, Leading power accuracy in lattice calculations of parton distributions, Phys. Lett. B **844**, 138081 (2023).
[47] J.-H. Zhang, J.-W. Chen, X. Ji, L. Jin, and H.-W. Lin, Pion distribution amplitude from lattice QCD, Phys. Rev. D **95**, 094514 (2017).
[48] G. S. Bali, V. M. Braun, B. Gläßle, M. Göckeler, M. Gruber, F. Hutzler, P. Korcyl, A. Schäfer, P. Wein, and J.-H. Zhang, Pion distribution amplitude from Euclidean correlation functions: Exploring universality and higher-twist effects, Phys. Rev. D **98**, 094507 (2018).
[49] J. Xu, Q.-A. Zhang, and S. Zhao, Light-cone distribution amplitudes of vector meson in a large momentum effective theory, Phys. Rev. D **97**, 114026 (2018).
[50] J.-H. Zhang, L. Jin, H.-W. Lin, A. Schäfer, P. Sun, Y.-B. Yang, R. Zhang, Y. Zhao, and J.-W. Chen, Kaon distribution amplitude from lattice QCD and the flavor SU(3) symmetry, Nucl. Phys. **B939**, 429 (2019).
[51] Y.-S. Liu, W. Wang, J. Xu, Q.-A. Zhang, S. Zhao, and Y. Zhao, Matching the meson quasidistribution amplitude in the RI/MOM scheme, Phys. Rev. D **99**, 094036 (2019).
[52] W. Wang, Y.-M. Wang, J. Xu, and S. Zhao, B-meson light-cone distribution amplitude from Euclidean quantities, Phys. Rev. D **102**, 011502 (2020).
[53] R. Zhang, C. Honkala, H.-W. Lin, and J.-W. Chen, Pion and kaon distribution amplitudes in the continuum limit, Phys. Rev. D **102**, 094519 (2020).
[54] J. Hua, M.-H. Chu, P. Sun, W. Wang, J. Xu, Y.-B. Yang, J.-H. Zhang, and Q.-A. Zhang, Distribution amplitudes of $K^*$ and $\phi$ at the physical pion mass from lattice QCD, Phys. Rev. Lett. **127**, 062002 (2021).
[55] J. Hua *et al.*, Pion and kaon distribution amplitudes from lattice QCD, Phys. Rev. Lett. **129**, 132001 (2022).
[56] S.-M. Hu, W. Wang, J. Xu, and S. Zhao, Accessing the subleading-twist B-meson light-cone distribution amplitude with large-momentum effective theory, arXiv:2308.13977.
[57] X. Ji, P. Sun, X. Xiong, and F. Yuan, Soft factor subtraction and transverse momentum dependent parton distributions on the lattice, Phys. Rev. D **91**, 074009 (2015).
[58] X. Ji, L.-C. Jin, F. Yuan, J.-H. Zhang, and Y. Zhao, Transverse momentum dependent parton quasidistributions, Phys. Rev. D **99**, 114006 (2019).
[59] X. Ji, Y. Liu, and Y.-S. Liu, Transverse-momentum-dependent parton distribution functions from large-momentum effective theory, Phys. Lett. B **811**, 135946 (2020).
[60] X. Ji, Y. Liu, and Y.-S. Liu, TMD soft function from large-momentum effective theory, Nucl. Phys. **B955**, 115054 (2020).
[61] M. A. Ebert, I. W. Stewart, and Y. Zhao, Towards quasi-transverse momentum dependent PDFs computable on the lattice, J. High Energy Phys. 09 (2019) 037.
[62] M. A. Ebert, S. T. Schindler, I. W. Stewart, and Y. Zhao, One-loop matching for spin-dependent quasi-TMDs, J. High Energy Phys. 09 (2020) 099.
[63] X. Ji, Y. Liu, and Y.-S. Liu, Transverse-momentum-dependent parton distribution functions from large-momentum effective theory, Phys. Lett. B **811**, 135946 (2020).
[64] P. Shanahan, M. Wagman, and Y. Zhao, Lattice QCD calculation of the Collins-Soper kernel from quasi-TMDPDFs, Phys. Rev. D **104**, 114502 (2021).
[65] Q.-A. Zhang *et al.*, Lattice-QCD calculations of TMD soft function through large-momentum effective theory, Phys. Rev. Lett. **125**, 192001 (2020).
[66] Y. Li *et al.*, Lattice QCD study of transverse-momentum dependent soft function, Phys. Rev. Lett. **128**, 062002 (2022).
[67] S. T. Schindler, I. W. Stewart, and Y. Zhao, One-loop matching for gluon lattice TMDs, J. High Energy Phys. 08 (2022) 084.
[68] K. Zhang, X. Ji, Y.-B. Yang, F. Yao, and J.-H. Zhang, Renormalization of transverse-momentum-dependent parton distribution on the lattice, Phys. Rev. Lett. **129**, 082002 (2022).
[69] R. Zhu, Y. Ji, J.-H. Zhang, and S. Zhao, Gluon transverse-momentum-dependent distributions from large-momentum effective theory, J. High Energy Phys. 02 (2023) 114.
[70] J.-C. He, M.-H. Chu, J. Hua, X. Ji, A. Schäfer, Y. Su, W. Wang, Y. Yang, J.-H. Zhang, and Q.-A. Zhang, Unpolarized transverse-momentum-dependent parton distributions of the nucleon from lattice QCD, arXiv:2211.02340.
[71] M.-H. Chu *et al.*, Lattice calculation of the intrinsic soft function and the Collins-Soper kernel, J. High Energy Phys. 08 (2023) 172.
[72] Y. Zhao, Transverse momentum distributions from lattice QCD without Wilson lines, arXiv:2311.01391.
[73] X. Ji, A. Schäfer, X. Xiong, and J.-H. Zhang, One-loop matching for generalized parton distributions, Phys. Rev. D **92**, 014039 (2015).
[74] Y.-S. Liu, W. Wang, J. Xu, Q.-A. Zhang, J.-H. Zhang, S. Zhao, and Y. Zhao, Matching generalized parton quasidistributions in the RI/MOM scheme, Phys. Rev. D **100**, 034006 (2019).

[75] J.-W. Chen, H.-W. Lin, and J.-H. Zhang, Pion generalized parton distribution from lattice QCD, Nucl. Phys. **B952**, 114940 (2020).
[76] C. Alexandrou, K. Cichy, M. Constantinou, K. Hadjiyiannakou, K. Jansen, A. Scapellato, and F. Steffens, Unpolarized and helicity generalized parton distributions of the proton within lattice QCD, Phys. Rev. Lett. **125**, 262001 (2020).
[77] H.-W. Lin, Nucleon tomography and generalized parton distribution at physical pion mass from lattice QCD, Phys. Rev. Lett. **127**, 182001 (2021).
[78] C. Alexandrou, K. Cichy, M. Constantinou, K. Hadjiyiannakou, K. Jansen, A. Scapellato, and F. Steffens, Generalized parton distributions of the proton from lattice QCD, Proc. Sci. LATTICE2021 (**2022**) 129 [arXiv:2111.03226].
[79] J. Dodson, S. Bhattacharya, K. Cichy, M. Constantinou, A. Metz, A. Scapellato, and F. Steffens, First lattice QCD study of proton twist-3 GPDs, Proc. Sci. LATTICE2021 (**2022**) 054 [arXiv:2112.05538].
[80] C. Alexandrou, K. Cichy, M. Constantinou, K. Hadjiyiannakou, K. Jansen, A. Scapellato, and F. Steffens, Transversity GPDs of the proton from lattice QCD, Phys. Rev. D **105**, 034501 (2022).
[81] A. Scapellato, C. Alexandrou, K. Cichy, M. Constantinou, K. Hadjiyiannakou, K. Jansen, and F. Steffens, Proton generalized parton distributions from lattice QCD, Rev. Mex. Fis. Suppl. **3**, 0308104 (2022) [arXiv:2201.06519].
[82] J. P. Ma, Z. Y. Pang, C. P. Zhang, and G. P. Zhang, QCD factorization of quasi generalized gluon distributions, J. High Energy Phys. 04 (2023) 001.
[83] S. Bhattacharya, K. Cichy, M. Constantinou, J. Dodson, A. Metz, A. Scapellato, and F. Steffens, Chiral-even axial twist-3 GPDs of the proton from lattice QCD, Phys. Rev. D **108**, 054501 (2023).
[84] X. Ji and Y. Liu, Computing light-front wave functions without light-front quantization: A large-momentum effective theory approach, Phys. Rev. D **105**, 076014 (2022).
[85] Z.-F. Deng, W. Wang, and J. Zeng, Transverse-momentum-dependent wave functions and soft functions at one-loop in large momentum effective theory, J. High Energy Phys. 09 (2022) 046.
[86] M.-H. Chu, Collins-Soper kernel from transverse momentum-dependent wave functions in LaMET, Proc. Sci. LATTICE2021 (**2022**) 424.
[87] M.-H. Chu *et al.*, Nonperturbative determination of the Collins-Soper kernel from quasitransverse-momentum-dependent wave functions, Phys. Rev. D **106**, 034509 (2022).
[88] M.-H. Chu *et al.*, Transverse-momentum-dependent wave functions of pion from lattice QCD, arXiv:2302.09961.
[89] J.-H. Zhang, Double parton distributions from Euclidean lattice, arXiv:2304.12481.
[90] M. Jaarsma, R. Rahn, and W. J. Waalewijn, Towards double parton distributions from first principles using large momentum effective theory, J. High Energy Phys. 12 (2023) 014.
[91] K. Cichy and M. Constantinou, A guide to light-cone PDFs from lattice QCD: An overview of approaches, techniques and results, Adv. High Energy Phys. **2019**, 3036904 (2019).
[92] Y. Zhao, Unraveling high-energy hadron structures with lattice QCD, Int. J. Mod. Phys. A **33**, 1830033 (2019).
[93] K. Orginos, A. Radyushkin, J. Karpie, and S. Zafeiropoulos, Lattice QCD exploration of parton pseudo-distribution functions, Phys. Rev. D **96**, 094503 (2017).
[94] A. V. Radyushkin, Quasi-parton distribution functions, momentum distributions, and pseudo-parton distribution functions, Phys. Rev. D **96**, 034025 (2017).
[95] A. V. Radyushkin, Quark pseudodistributions at short distances, Phys. Lett. B **781**, 433 (2018).
[96] V. Braun, P. Gornicki, and L. Mankiewicz, Ioffe-time distributions instead of parton momentum distributions in description of deep inelastic scattering, Phys. Rev. D **51**, 6036 (1995).